PERGAMON

International Journal of Solids and Structures 38 (2001) 1281–1293

INTERNATIONAL JOURNAL OF SOLIDS and STRUCTURES

www.elsevier.com/locate/ijsolstr

Rigid square inclusion embedded within an epoxy disk: asymptotic stress analysis

E.D. Reedy Jr. *, T.R. Guess

Sandia National Laboratories, Albuquerque NM 87185, USA

Received 6 February 1999; in revised form 9 March 2000

Abstract

The asymptotically singular stress state found at the tip of a rigid, square inclusion embedded within a thin, linear elastic disk has been determined for both uniform cooling and an externally applied pressure. Since these loadings are symmetric, the singular stress field is characterized by a single stress intensity factor K_a, and the applicable K_a calibration relationship has been determined for both a fully bonded inclusion and an unbonded inclusion with frictionless sliding. A lack of interfacial bonding has a profound effect on inclusion-tip stress fields. When the inclusion is fully bonded, radial compression dominates in the region directly in front of the inclusion tip and there is negligible tensile hoop stress. When the inclusion is unbonded the radial stress at the inclusion tip is again compressive, but now the hoop tensile stress is of equal magnitude. Consequently, an epoxy disk containing an unbonded inclusion appears to be more likely to crack when cooled than a disk containing a fully bonded inclusion. Elastic–plastic calculations show that when the inclusion is unbonded, encapsulant yielding has a significant effect on the inclusion-tip stress state. Yielding relieves stress parallel to the interface and greatly reduces the radial compressive stress in front of the inclusion. As a result, the encapsulant is subjected to a nearly uniaxial tensile stress at the inclusion tip. For a typical high-strength epoxy, the calculated yield zone is embedded within the region dominated by the elastic hoop stress singularity. A limited number of tests have been carried out to determine if encapsulant cracking can be induced by cooling a specimen fabricated by molding a square, steel insert within a thin epoxy disk. Test results are in qualitative agreement with analysis. Cracks developed only in disks with mold-released inserts, and the tendency for cracking increased with inclusion size. © 2001 Published by Elsevier Science Ltd.

Keywords: Corner; Cracking; Epoxy; Fracture; Inclusion; Stress singularity; Stress intensity factor

1. Introduction

Polymeric encapsulants are widely used in the automotive, aerospace, and electronic industries. The encapsulant holds a component in place and protects it from applied loads and the surrounding environment. If the encapsulant cracks the component may fail. In many cases the encapsulated part has sharp corners. For example, sharp corners are often found in microelectronic chip packages. When failure occurs,

* Corresponding author. Fax: +1-505-844-9297.
E-mail address: edreedy@sandia.gov (E.D. Reedy Jr.).

0020-7683/01/$ - see front matter © 2001 Published by Elsevier Science Ltd.
PII: S0020-7683(00)00087-1

it will typically initiate at a corner. On a finer scale, polymer encapsulants are usually filled with particles to improve their properties. Some common types of fillers are created by crushing a bulk material, and as a consequence, the filler has sharp corners. Microcracks initiating at sharp-cornered particles can degrade a filled material.

A simple, 2-D idealization of an encapsulated sharp-cornered component or particle is a homogeneous, isotropic, square inclusion embedded within an isotropic material (Fig. 1). The encapsulated component or particle is typically much stiffer than the encapsulant, and it is often reasonable to regard the inclusion as rigid. When viewed asymptotically, the inclusion tip is the apex of a wedge (Fig. 2). Several studies have provided detailed information about the stress field found at the tip of a linear elastic wedge. Williams (1952) analyzed a single material wedge with a variety of edge boundary conditions. He noted that a power-law stress singularity

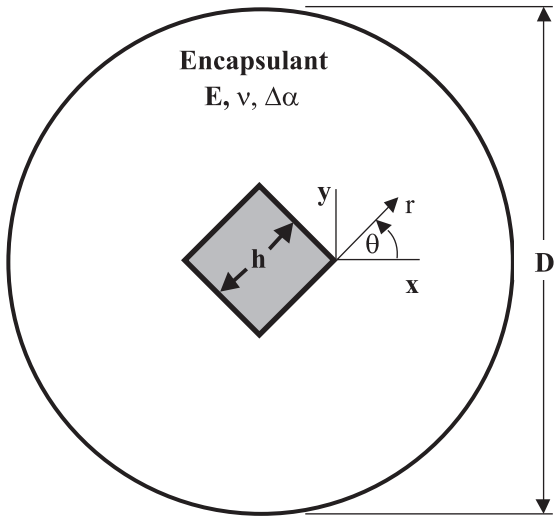

Fig. 1. Rigid, square inclusion encapsulated within a linear elastic disk.

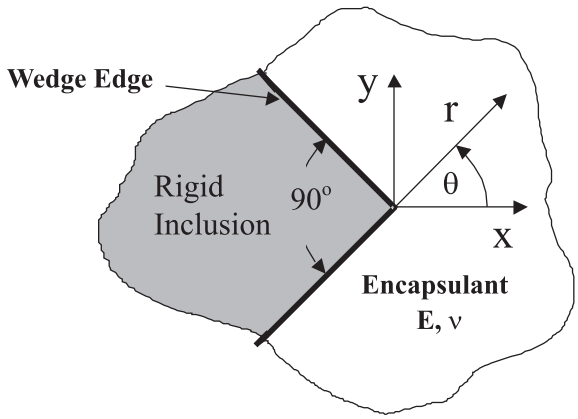

Fig. 2. Asymptotic problem for encapsulated, rigid wedge. Symmetry about the x-axis.

$$\sigma \sim K_a r^{\lambda-1}, \quad -1 < \mathrm{Re}(\lambda - 1) < 0 \tag{1}$$

can exist at the apex of the wedge and determined how the order of the stress singularity, $\lambda - 1$, depends on boundary conditions and elastic properties. For singular stress and bounded displacements, $-1 < \mathrm{Re}(\lambda - 1) < 0$. Williams' results for a wedge with both edges clamped are applicable to a rigid inclusion surrounded by an elastic material. Bogy and Wang (1971) analyzed bonded, dissimilar elastic wedges that together form a full plane. These results show how the strength of the stress singularity depends on the elastic properties of the inclusion. Chen and Nisitani (1993) noted that there are at most two power-law singular terms in the asymptotic expansion of the stress field with $-1 < \lambda - 1 < 0$ for many cases of practical interest (when $\beta(\alpha - \beta) > 0$, where α, β are the elastic bimaterial parameters defined by Dundurs (1969)). The exponent defining the strength of each of the singular terms is real, and the two exponents are generally different. They also found that one of the singular terms is associated with symmetric loading about the line bisecting the apex of the wedge, whereas the other is associated with an asymmetric loading about the bisecting line (i.e., x-axis in Fig. 2). In another study, Chen (1994) presented stress intensity factor relations for a bonded inclusion embedded within an infinite plate subjected to uniaxial tension, biaxial tension or shear at infinity. A variety of inclusion shapes were considered.

The value of the stress intensity factor K_a (Eq. (1)) characterizes the magnitude of the stress state in the region of the inclusion tip (the subscript "a" on K is used to denote that this stress intensity factor is associated with the apex of a wedge). It is reasonable to hypothesize that failure occurs at a critical K_a value, K_{ac}. Such an approach is analogous to linear elastic fracture mechanics, except here the critical value of the stress intensity factor is associated with a discontinuity other than a crack. As is the case of linear elastic fracture mechanics, small-scale yielding conditions must apply. The asymptotic stress state characterized by K_a must dominate a region that is significantly larger than the fracture process zone, plastic yield zone, and the extent of any subcritical cracking. The inclusion tip must also appear sharp on this length scale.

The applicability and accuracy of a K_a-based failure analysis to encapsulated inclusions is yet to be conclusively demonstrated. There appear to be few published experimental results applying this approach to encapsulated bodies. One exception is the work of Hattori et al. (1989), who molded epoxy models with small Fe–Ni inserts and looked for failure as the molding cooled. Note, however, there is convincing evidence that the stress intensity factor for other types of corner discontinuity can be used to predict failure. Reedy and Guess (1993, 1995, 1996, 1997, and 1999) have shown that the observed reduction in the tensile strength of adhesively-bonded, cylindrical butt joints with increasing bond thickness is accurately predicted by a K_{ac} criterion. In this case K_{ac} is associated with an interface corner, the point where the interface between two bonded quarter planes intersects the stress-free edge. Dunn et al. (1997a,b) have successfully predicted the fracture of homogenous materials containing a sharp notch using a similar approach.

Reported below is the K_a calibration for a rigid, square inclusion embedded within a thin disk and subjected to either a uniform cooling or to an external applied pressure. This symmetrically loaded configuration is a particularly attractive test specimen, as the asymptotic stress field is characterized by a single K_a. Two extremes in bonding are considered: fully bonded and unbonded with frictionless sliding. Elastic–plastic calculations for a representative epoxy encapsulant have also been carried out. These results illustrate the effect of yielding on inclusion-tip stress fields and also the validity of the small-scale yielding assumption. Finally, the results of a limited number of preliminary experiments are presented.

2. Asymptotic solutions for bonded and unbonded inclusions

Fig. 1 shows the encapsulated-inclusion geometry analyzed. A rigid, square inclusion, with side length h, is embedded within a disk of diameter D. The disk is presumed thin relative to the characteristic inclusion dimension h, and a plane stress analysis is applied. Fig. 2 shows the associated asymptotic problem. Note

that there is a geometric symmetry about the x-axis and that the uniform cooling and applied pressure loadings considered in this study are also symmetric about the x-axis. Accordingly, the line bisecting the apex of the wedge (i.e., x-axis) is a line of symmetry. Furthermore, for plane stress and with the elastic encapsulant (with Young's modulus E and Poisson's ratio v) taken to be Material 1 and the rigid inclusion Material 2, Dundurs' (1969) elastic bimaterial parameters α, β take on the values $\alpha = -1$, and $\beta = -(1-v)/2$ and $\beta(\alpha-\beta) > 0$. Consequently, the asymptotic solution contains one singular term, and the singularity exponent is real (Chen and Nisitani, 1993, as discussed above in Section 1).

One anticipates that the nature of the inclusion-to-encapsulant bond has a substantial effect on inclusion-tip stress fields. Typically, a strong interfacial bond is sought, although a less-than-perfect encapsulation process could thwart this desire. Even when an inclusion is initially well bonded, that bond could fail with cyclic loading or from environmental attack. For this reason asymptotic results for a fully bonded inclusion are compared with those for an unbonded inclusion (i.e., mold released) that is free to undergo frictionless slip. When the inclusion is rigid, only the one-material wedge representing the encapsulant is analyzed. The edge boundary conditions are chosen to reflect the presence of the rigid inclusion. For a bonded inclusion the wedge edges are fully fixed. For an unbonded inclusion with frictionless slip, the edges are shear-free, and only the normal displacement is fixed. Here it is assumed that for uniform cooling ($\Delta T < 0$) or for a uniform external pressure ($P^* > 0$), interfacial normal stress is always compressive, and there is no tendency for a gap to form at the encapsulant-to-inclusion interface (this was verified by the finite element calculation discussed below). The homogeneous boundary conditions on the edges of the wedge define an eigenvalue problem for the strength of the stress singularity, and the angular variation of the asymptotic stress field is associated with the corresponding eigenfunctions. Solutions to these types of asymptotic problems are well known (Williams, 1952; Seweryn and Molski, 1996), so only the results are presented here.

Fig. 3 shows that the strength of the stress singularity displays a modest dependence on Poisson's ratio when the inclusion is fully bonded. When $v = 0.0$, $\lambda - 1 = -0.28$, whereas when $v = 0.5$, $\lambda - 1 = -0.23$. The severity of the stress singularity decreases as Poisson's ratio increases. This can be contrasted with the case of bonded rigid and elastic quarter planes (asymptotic problem for a butt joint), where the strength of the singularity vanishes when $v = 0.0$ and is maximum when $v = 0.5$ (Reedy, 1990). When the inclusion is unbonded, $\lambda - 1 = -0.67$; and this value does not vary with Poisson's ratio. The most notable finding is the dramatic increase in the strength of the stress singularity with interfacial debonding. The rigid inclusion

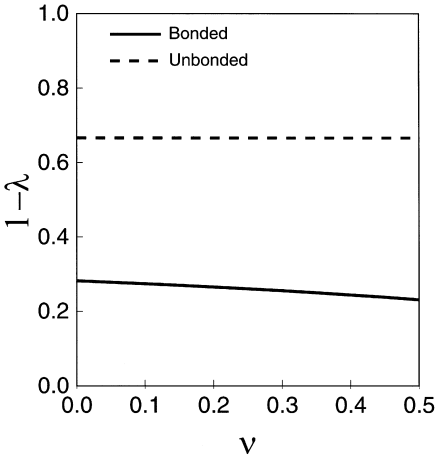

Fig. 3. Variation of the strength of the stress singularity, $-(1-\lambda)$, with Poisson's ratio v for either a bonded or an unbonded rigid square inclusion.

assumption is thought to be a reasonable representation of bimaterial combinations, such as a steel inclusion embedded within an epoxy encapsulant. Chen and Nisitani (1993) have determined the characteristic equation defining the order of the inclusion-tip stress singularity for a bonded elastic inclusion. This permits an assessment of the rigid inclusion assumption. The strength of the symmetric mode singularity for a fully bonded, square, steel inclusion ($E = 193$ GPa, $\nu = 0.3$) in epoxy ($E = 3.5$ GPa, $\nu = 0.35$) is -0.242, whereas that for a rigid inclusion is -0.250; only a 3% difference.

Not only is the strength of the stress singularity altered by debonding, but there is also a striking change in the angular variation of the asymptotic stress state. The spatial distribution of stress in the region dominated by the stress singularity is defined by

$$\sigma_{\alpha\beta} = K_a r^{\lambda-1} \bar{\sigma}_{\alpha\beta}(\theta) \quad (\alpha, \beta = r, \theta). \tag{2}$$

The functions defining the angular variation in the asymptotic stress components, $\bar{\sigma}_{rr}(\theta)$, $\bar{\sigma}_{\theta\theta}(\theta)$, and $\bar{\sigma}_{r\theta}(\theta)$, are plotted for a bonded ($\nu = 0.35$) and an unbonded inclusion in Figs. 4 and 5, respectively. Note that the

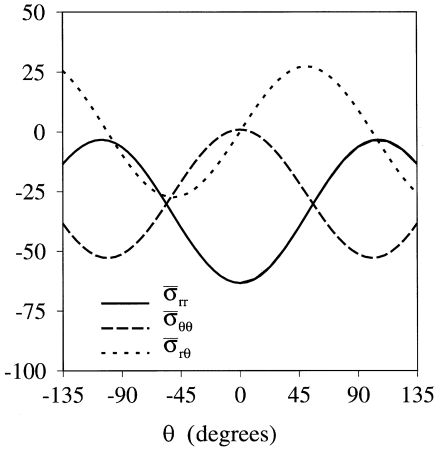

Fig. 4. Angular variation of σ_{rr}, $\sigma_{\theta\theta}$ and $\sigma_{r\theta}$ about the tip of a fully bonded, rigid square inclusion (encapsulant $\nu = 0.35$).

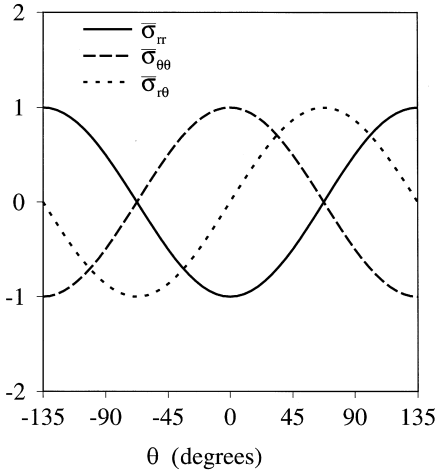

Fig. 5. Angular variation of σ_{rr}, $\sigma_{\theta\theta}$, and $\sigma_{r\theta}$ about the tip of an unbonded, rigid square inclusion (frictionless sliding).

functions are normalized so that $\bar{\sigma}_{\theta\theta}(0^\circ) = 1$. With this normalization the singular hoop stress directly in front of the inclusion tip $\sigma_{\theta\theta}(0^\circ) = K_a r^{\lambda-1}$. Fig. 4 shows that when the inclusion is fully bonded, the magnitude of the radial stress in front of inclusion tip ($\theta = 0^\circ$) is much larger than the hoop stress and differs in sign. On the other hand, Fig. 5 shows that when the inclusion is unbonded, hoop and radial stresses are again of opposite sign but of equal magnitude. Another indication of the profound difference in the asymptotic stress state of the bonded and unbonded inclusion is evident from a comparison of the functions defining the angular variation in pressure and effective stress (Figs. 6 and 7). Fig. 6 shows that effective stress $\sigma_e = (3J_2)^{1/2}$, where J_2 is the second stress deviator invariant, is highest in front of the inclusion tip, and the pressure component is roughly one third of the effective stress. When the inclusion is unbonded, the effective stress is singular but independent of angular position, and pressure is nonsingular.

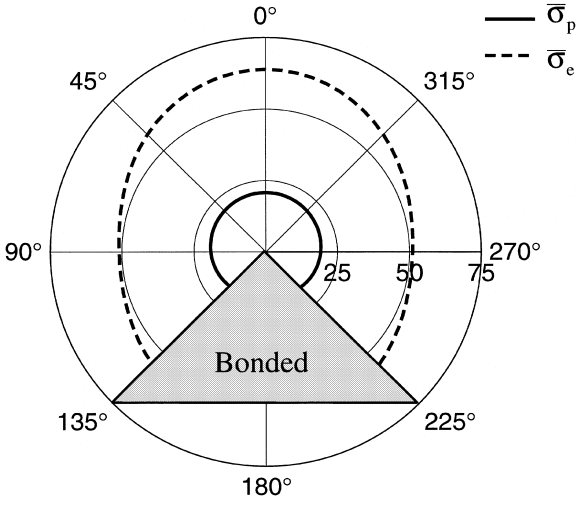

Fig. 6. Angular variation of σ_p and σ_e about the tip of a fully bonded, rigid square inclusion (encapsulant $\nu = 0.35$).

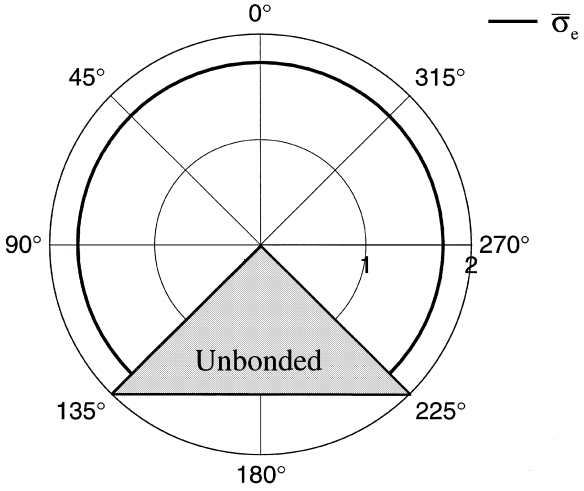

Fig. 7. Angular variation of σ_e about the tip of an unbonded, rigid square inclusion (frictionless sliding).

3. Calibration for inclusion-tip stress intensity factor K_a

Both the strength of the stress singularity, $\lambda - 1$, and the functions defining the angular variation in stress, $\bar{\sigma}_{\alpha\beta}(\theta)$, are fully determined by the asymptotic analysis. In contrast the inclusion-tip stress intensity factor K_a is determined by the full solution and depends on elastic properties, overall geometry, and the loading. Two axisymmetric (θ-independent) loadings are considered: uniform cooling ($\Delta T < 0$) and a uniform pressure ($P^* > 0$) applied to the disk's outer edge. These loadings are actually related. The solution for uniform cooling can be obtained by superposing a suitably chosen constant stress state with the solution for an applied pressure. If the outer edge of the epoxy disk is fixed and the disk is subjected to a uniform temperature change ΔT, then the plane stress solution is $\varepsilon_{rr} = \varepsilon_{\theta\theta} = 0$, and $\sigma_{rr} = \sigma_{\theta\theta} = -E\Delta\alpha\Delta T/(1-\nu)$, where $\Delta\alpha$ is the differential coefficient of thermal expansion ($\Delta\alpha$ = encapsulant CTE–inclusion CTE). This solution is valid for both bonded and unbonded inclusions. The superposition of this constant stress state and the solution for a disk subjected to an edge pressure $P^* = -E\Delta\alpha\Delta T/(1-\nu)$ yields the solution for the uniform cooling of a disk with a stress-free edge. The pressure loading provides the fundamental singular solution, and the magnitude of the stress singularity will depend on P^*, with $P^* = -E\Delta\alpha\Delta T/(1-\nu)$ for uniform cooling.

The region dominated by the asymptotic solution can be extended by adding an asymptotically constant term, when it exists, to the singular term (Reedy, 1993). The asymptotic solution then has the form

$$\sigma_{\alpha\beta} = K_a r^{\lambda-1}\bar{\sigma}_{\alpha\beta}(\theta) + C\delta_{\alpha\beta} \quad (\alpha,\beta = r,\theta). \tag{3}$$

The constant stress term C must satisfy the asymptotic boundary conditions and for simple cases is readily determined. For example, consider a uniformly cooled encapsulant bonded to a rigid inclusion. If the encapsulant were unbonded, its in-plane area would change with a change in temperature (i.e., free thermal expansion). In a plane stress analysis, the stress state $\sigma^* = \sigma_{rr} = \sigma_{\theta\theta} = -E\Delta\alpha\Delta T/(1-\nu)$ produces an area change that precisely negates that of the thermal expansion. Consequently, this constant stress state satisfies the asymptotic problem of a uniformly cooled encapsulant bonded to a rigid inclusion (fixed edges) since the total strain is zero. Yang and Munz (1995) have determined the asymptotic constant stress term for the more general case of a two-material elastic joint subjected to a uniform temperature change, and their result reduces to that presented here for the rigid inclusion.

Based upon dimensional considerations and the required linear dependence on load, the inclusion-tip K_a calibration relation must have the form

$$K_a = \sigma^* h^{1-\lambda} I_p\left(\nu, \frac{D}{h}\right), \tag{4}$$

where

$$\sigma^* = \begin{cases} P^*, & \text{uniform applied pressure } P^*, \\ \frac{-E\Delta\alpha\Delta T}{(1-\nu)}, & \text{uniform temperature change } \Delta T, \end{cases} \tag{5}$$

whereas the asymptotically constant term is

$$C = \begin{cases} \frac{-E\Delta\alpha\Delta T}{(1-\nu)}, & \text{bonded rigid inclusion}, \\ -P^*, & \text{unbonded rigid inclusion}. \end{cases} \tag{6}$$

Note that for a bonded inclusion, $C = 0$ when $\Delta T = 0$ and $P^* \neq 0$, whereas for an unbonded inclusion, $C = 0$ when $P^* = 0$ and $\Delta T \neq 0$. The function I_p depends on nondimensional material and geometric parameters, and for this problem the only possibilities are ν and D/h. The value of I_p for ν and D/h combinations of interest can be determined by matching asymptotic and full field, finite element solutions.

Fig. 8 shows a typical mesh used in the finite element calculations. Only one eighth of the disk (Fig. 1) is analyzed. The loading is symmetric, and there is geometric symmetry about the x and y axes as well as

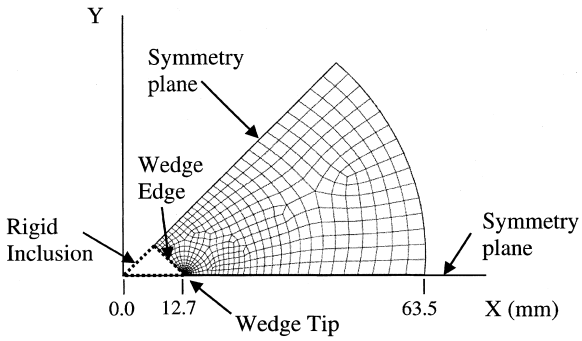

Fig. 8. Typical finite element mesh used in analysis.

about the two lines that divide the square inclusion into four smaller squares. Bonded and unbonded inclusions are modeled by applying the appropriate boundary conditions to the wedge edge. A highly refined mesh is used in the region of the inclusion tip (smallest element $/ h = 1.4 \times 10^{-5}$) to ensure an accurate match with the asymptotic solution. The mesh is composed of four-noded, plane stress elements. A calculation must be carried out for every v and D/h combination of interest (h and σ^* can be arbitrarily chosen). For the case of the unbonded inclusion, hoop stress along the x-axis is used to calculate K_a (Eq. (3)), and then Eq. (4) is used to determine I_p. When the inclusion is bonded, the magnitude of the radial stress component along the x-axis is significantly higher than that of the hoop component (Fig. 9). Consequently, when the inclusion is bonded, the radial stress along the x-axis (with the asymptotic constant term that exists in this case subtracted out) is used to calculate K_a and I_p. Table 1 lists $\lambda - 1$ and I_p values for a range of v and D/h. Note that results for the unbonded inclusion display only a minimal dependence on D/h for $D/h > 5$. For this range of D/h, the stress state is essentially independent of D (i.e., disk acts as if its infinite).

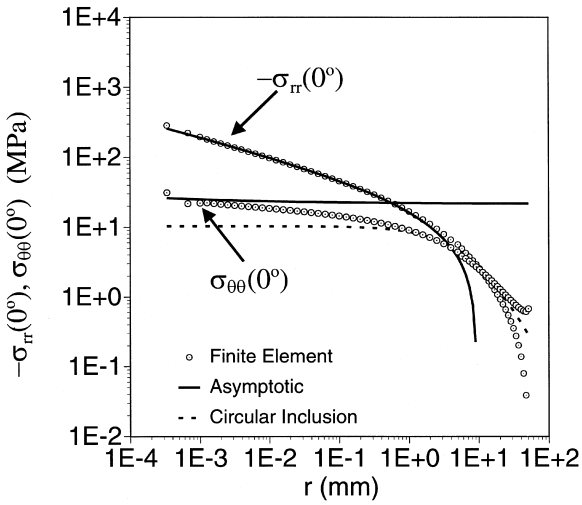

Fig. 9. Comparison of linear elastic finite element and asymptotic solutions for stress in front of a fully bonded inclusion embedded within an epoxy disk with $h = 18$ mm and $\Delta T = -100°C$.

Table 1
Value of $\lambda - 1$ and I_p for various v and D/h

Interface	v	D/h	$\lambda - 1$	$\bar{\sigma}_{rr}(0^\circ)$	$\bar{\sigma}_{\theta\theta}(0^\circ)$	I_p
Bonded	0.35	7.07	−0.2502	−63.25	1.00	0.0135
Unbonded	0.05	14.14	−0.6667	−1.00	1.00	0.1779
Unbonded	0.15	14.14	−0.6667	−1.00	1.00	0.1455
Unbonded	0.25	14.14	−0.6667	−1.00	1.00	0.1182
Unbonded	0.35	14.14	−0.6667	−1.00	1.00	0.0949
Unbonded	0.45	14.14	−0.6667	−1.00	1.00	0.0748
Unbonded	0.35	7.07	−0.6667	−1.00	1.00	0.0940
Unbonded	0.35	5.66	−0.6667	−1.00	1.00	0.0935
Unbonded	0.35	4.71	−0.6667	−1.00	1.00	0.0927
Unbonded	0.35	3.54	−0.6667	−1.00	1.00	0.0910
Unbonded	0.35	2.83	−0.6667	−1.00	1.00	0.0886
Unbonded	0.35	2.18	−0.6667	−1.00	1.00	0.0831

For a sufficiently large D/h it seems likely that the stress state developed in regions far from the inclusion will not depend on inclusion shape. The stresses are expected to approach those found in a disk containing a circular inclusion of equal area. Specifically for $r \gg h$, one anticipates for plane stress

$$\sigma_{rr} = -\sigma_{\theta\theta} = \frac{E\Delta\alpha\Delta T}{1+v}\left(\frac{r_0}{r}\right)^2, \quad \text{where } r_0 = \frac{h}{\sqrt{\pi}}. \tag{7}$$

4. Comparison of full and asymptotic solutions

The results plotted in Figs. 9 and 10 illustrate the nature of inclusion-tip stress fields and the range of applicability of the asymptotic solutions. These results are for a disk with diameter $D = 127$ mm and for an

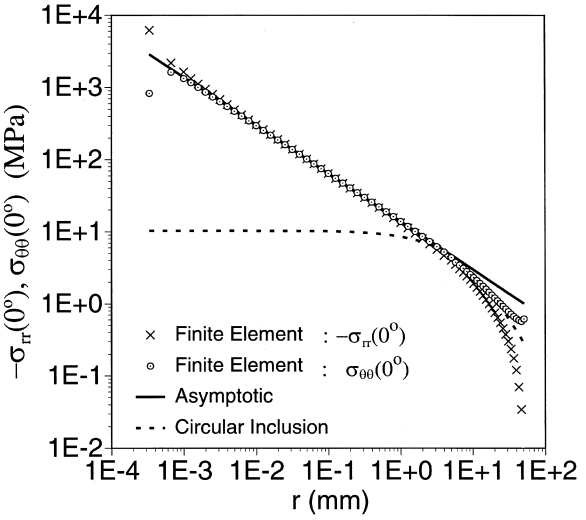

Fig. 10. Comparison of linear elastic finite element and asymptotic solutions for stress in front of an unbonded inclusion embedded within an epoxy disk with $h = 18$ mm and $\Delta T = -100^\circ$C.

inclusion with side length $h = 18$ mm ($D/h = 7$). The disk is subjected to uniform cooling with $\Delta T = -100$°C. Encapsulant properties are representative of a typical, high-strength epoxy. The encapsulant has a Young's modulus $E = 3.5$ GPa, Poisson's ratio $\nu = 0.35$, and $\Delta\alpha = 40 \times 10^{-6}/$°C.

When cooled, a large radial compressive stress is generated at the tip of a bonded inclusion (Fig. 9). Although tensile, the hoop stress is relatively low. This stress state does not seem to favor encapsulant cracking. Recall that for the bonded inclusion, an asymptotically constant term exists whenever $\Delta T \neq 0$ (Eq. 6). This term must be added to the singular term to get good agreement with the finite element result. When the constant term is included, the asymptotic and finite element results for $\sigma_{rr}(0°)$ are within 4% for $r/h < 0.056$. The finite element and circular inclusion results for $\sigma_{rr}(0°)$ merge when $r/h > 0.2$. A large tensile hoop stress is generated when a disk with an unbonded inclusion is cooled and, consequently, could promote cracking (Fig. 10). The radial stress is of equal magnitude but is compressive. The asymptotic solution contains only a singular term, and it is within 4% of the finite element result when $r/h < 0.17$. When combined, the asymptotic and circular inclusion solutions provide an excellent match to the finite element solution over the full range of r/h. Since a large tensile hoop stress is generated only when the inclusion is unbonded, one might speculate that for encapsulant cracking to initiate at the tip of a well-bonded inclusion, the inclusion tip may need to first debond. Such debonding could be produced by thermal cycling or perhaps by environmental weakening of the interface.

Figs. 11 and 12 illustrate the effect of encapsulant yielding on inclusion-tip stress fields. The epoxy is idealized as an elastic, perfectly plastic material ($\sigma_y = 74$ MPa). Although this is a reasonable idealization when the temperature is sufficiently below the epoxy's glass transition temperature, T_g, epoxy actually responds in a much more complex manner. Stress relaxation data suggest that epoxies display nonlinear, stress-dependent viscoelasticity, and yielding is a manifestation of this constitutive behavior (Reedy and Guess, 1996). When the inclusion is fully bonded, the calculated yield zone is 0.013 mm long (at $\theta = 0°$, see Fig. 11). When the inclusion is unbonded, the yield zone is ten times longer (Fig. 12). Yielding substantially alters the stress state at the tip of the unbonded inclusion. Yielding relieves stress parallel to the interface and greatly reduces the magnitude of the radial compressive stress found in front of the inclusion. Consequently, the encapsulant directly in front of the inclusion is subjected to a nearly uniaxial, hoop tensile stress. Note that the yield zone is still embedded within the singular elastic field defining hoop stress and is, accordingly, characterized by K_a.

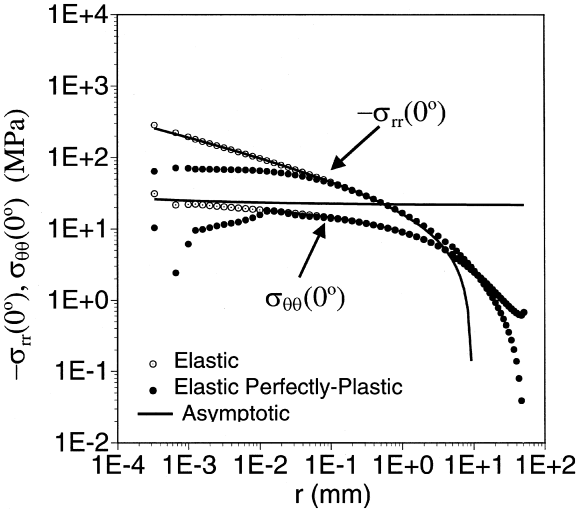

Fig. 11. Comparison of linear elastic and elastic, perfectly plastic finite element solutions with asymptotic solution for stress in front of a fully bonded inclusion embedded within an epoxy disk with $h = 18$ mm and $\Delta T = -100$°C.

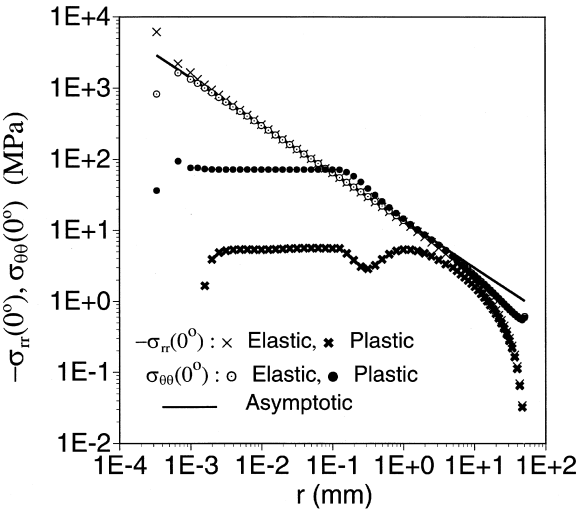

Fig. 12. Comparison of linear elastic and elastic-perfectly-plastic finite element solutions with asymptotic solution for stress in front of an unbonded inclusion embedded within an epoxy disk with $h = 18$ mm and $\Delta T = -100°C$.

5. Comparison with experiment

A limited number of encapsulated-inclusion specimens have been fabricated and tested. The primary goal was to simply determine if encapsulant cracking could be induced when cooling a reasonably sized specimen. Specimens were fabricated in an RTV mold. The inclusion was centered and then attached (using double-sided tape) to the bottom of a mold containing a 127 mm diameter, 6 mm deep cylindrical cavity. A lid, incorporating fill and bleed holes, ensured that the surfaces of the inclusion and epoxy disk were flush. An Epon 828 (digylcidyl ether of bisphenol A) cured with DEA (diethanolamine) epoxy was used for the encapsulant (100/12 mix ratio, cured for 16 hours at 70°C); and sharp-cornered, stainless steel inclusions, with an edge-length of either $h = 9$ or 18 mm, were encapsulated. In some cases a mold release was applied to the inclusion to simulate the unbonded condition.

A liquid-nitrogen cooled environmental chamber was used to test the specimens. The specimens were cooled at a rate of 1°C/min. Initial tests, using specimens with thermocouples mounted at several radial positions, showed that this rate produced nearly uniform cooling of the epoxy disk. Several specimens could be hung in the central part of the chamber at the same time. The temperature at crack initiation was determined by observing the specimens through a window in the environmental chamber. Two specimens with the larger inclusion ($h = 18$ mm) were fabricated and tested. One specimen contained an inclusion whose edges were mold-released, whereas the other specimen contained an inclusion whose edges were subjected to a light sandblast. The specimen with the mold-released inclusion failed when first cooled to $-70°C$. The crack initiated from the inclusion tip. The specimen with the good interfacial bond (sand-blasted edge) was cooled three separate times to $-80°C$ and once to $-140°C$ without encapsulant cracking. This result confirms the expectation that an unbonded inclusion promotes encapsulant cracking.

If encapsulant cracking occurs at a critical K_a value, then the temperature change required to initiate cracking decreases with increasing inclusion size (see Eq. (4)). Therefore, 10 additional specimens with mold-released inclusions were fabricated. Half of these specimens contained the larger inclusion ($h = 18$ mm) and the other half contained the smaller inclusion ($h = 9$ mm). Three specimens of each inclusion size were cooled to $-80°C$, and then held at that temperature for up to three hours. Encapsulant cracking occurred in only one of the six specimens. The specimen that cracked contained the larger inclusion ($h = 18$

mm), and cracking occurred during the −80°C hold. The four remaining specimens were first heated to 90°C (above the epoxy's T_g of 70°C), held at that temperature for about 30 min, and then cooled. Neither of the two specimens with the smaller inclusion cracked. On the other hand one of the specimens with the larger inclusion cracked at −105°C, and the other cracked at −135°C. In spite of the limit scope of the initial tests, the results obtained to date are in qualitative agreement with the analysis. Upon cooling, cracks developed only in disks with mold-released inclusions, and cracking occurred only in specimens with the larger inclusion.

6. Summary

The K_a calibration for a rigid, square inclusion embedded within a thin, epoxy disk and subjected to either a uniform cooling or to an external applied pressure has been determined. This symmetrically loaded configuration is a particularly attractive test specimen since the asymptotic stress field is characterized by a single K_a. Both fully bonded and unbonded (frictionless sliding) conditions were considered. Note that for the idealized, plane stress inclusion geometry analyzed:

(1) The singular stress state generated by the bonded inclusion is very different from that generated by the unbonded inclusion. For an encapsulant with a Poisson's ratio of 0.35, the strength of stress singularity for the bonded inclusion is −0.25, whereas the strength of the singularity for the unbonded inclusion is −0.67. The angular variation of the stress field also differs. When the inclusion is fully bonded, the magnitude of the radial stress in front of inclusion tip ($\theta = 0°$, Fig. 1) is much larger than the hoop stress. When the inclusion is unbonded, hoop and radial stress have the same magnitude but are of opposite sign.

(2) An epoxy disk with an unbonded inclusion appears to be more likely to crack when cooled than a disk containing a fully bonded inclusion. A large radial compressive stress is generated in front of the inclusion tip when the inclusion is fully bonded, whereas a large tensile hoop stress is generated when the inclusion is unbonded. One might speculate that for encapsulant cracking to initiate at the tip of an initially well-bonded inclusion, the inclusion tip might need to first debond. Such debonding could be generated by thermal cycling or perhaps by environmental weakening of the interface.

(3) Encapsulant yielding has a significant effect on the nature of the stress state at the tip of an unbonded inclusion. Yielding relieves stress parallel to the interface and greatly reduces the magnitude of the radial compressive stress found in front of the inclusion. Consequently, the encapsulant directly in front of the inclusion is subjected to a nearly uniaxial, tensile stress. For a typical high-strength epoxy, the calculated yield zone is embedded within the singular elastic field defining hoop stress and is accordingly characterized by K_a.

(4) Results of a very limited number of tests are in qualitative agreement with the analysis. A square, sharp-cornered steel insert was encapsulated within a thin, epoxy disk. Upon cooling, cracks developed only in disks with mold-released inserts. The likelihood for cracking is expected to increase with inclusion size, and only those disks with the largest inclusion cracked.

Acknowledgements

This work was performed at Sandia National Laboratories. Sandia is a multiprogram laboratory operated by Sandia Corporation, a Lockheed Martin Company, for the United States Department of Energy under Contract DE-AC04-94AL85000. Mark Stavig performed the embedded inclusion tests.

References

Bogy, D.B., Wang, K.C., 1971. Stress singularities at interface corners in bonded dissimilar isotropic elastic materials. International Journal of Solids and Structures 7, 993–1005.

Chen, D.-H., Nisitani, H., 1993. Singular stress field near the corner of jointed dissimilar materials. Journal of Applied Mechanics 60, 607–613.

Chen, D.-H., 1994. Analysis of singular stress field around the inclusion corner tip. Engineering Fracture Mechanics 49, 533–546.

Dundurs, J., 1969. Discussion of edge-bonded dissimilar orthogonal elastic wedges under normal and shear loading. Journal of Applied Mechanics 36, 650–652.

Dunn, M.L., Suwito, W., Cunningham, S., 1997a. Fracture initiation at sharp notches: correlation using critical stress intensities. International Journal of Solids and Structures 34, 3873–3883.

Dunn, M.L., Suwito, W., Cunningham, S., May, C.W., 1997b. Fracture initiation at sharp notches under mode I mode II and mild mixed mode loading. International Journal of Fracture 84, 367–381.

Hattori, T., Sakata, S., Murakami, G., 1989. A stress singularity parameter approach for evaluating the interfacial reliability of plastic encapsulated LSI devices. Journal of Electronic Packaging 111, 243–248.

Reedy Jr., E.D., 1990. Intensity of the stress singularity at the interface corner between a bonded elastic and rigid layer. Engineering Fracture Mechanics 36, 575–583.

Reedy Jr., E.D., 1993. Asymptotic interface corner solutions for butt tensile joints. International Journal of Solids and Structures 30, 767–777.

Reedy Jr., E.D., Guess, T.R., 1993. Comparison of butt tensile strength data with interface corner stress intensity factor prediction. International Journal of Solids and Structures 30, 2929–2936.

Reedy Jr., E.D., Guess, T.R., 1995. Butt joint tensile strength: interface corner stress intensity factor prediction. Journal of Adhesion Science and Technology 9, 237–251.

Reedy Jr., E.D., Guess, T.R., 1996. Butt joint strength: effect of residual stress and stress relaxation. Journal of Adhesion Science and Technology 10, 33–45.

Reedy Jr., E.D., Guess, T.R., 1997. Interface corner failure analysis of joint strength: effect of adherend stiffness. International Journal of Fracture 88, 305–314.

Reedy Jr., E.D., Guess, T.R., 1999. Additional interface corner toughness data for an adhesively-bonded butt joint. International Journal of Fracture 98, L3–L8.

Seweryn, A., Molski, K., 1996. Elastic stress singularities and corresponding generalized stress intensity factors for angular corners under various boundary conditions. Engineering Fracture Mechanics 55, 529–556.

Williams, M.L., 1952. Stress singularities resulting from various boundary conditions in angular corners of plates in extension. Journal of Applied Mechanics 19, 526–528.

Yang, Y.Y., Munz, D., 1995. Stress intensity factor and stress distribution in a joint with an interface corner under thermal and mechanical loading. Computers and Structures 57, 467–476.